

14. CHEMICAL COMPOSITIONS OF FERROMANGANESE MICRONODULES IN SEDIMENTS AT SITE 1216, ODP LEG 199, PALEOGENE EQUATORIAL TRANSECT¹

T. Ito,² K. Komuro,³ K. Hatsuya,³ and H. Nishi⁴

ABSTRACT

Distribution, size, mineral, and chemical compositions of ferromanganese micronodules (FMMNs) and chemical composition of host sediments were examined in a series of red clay samples with ages from Eocene to the present at Ocean Drilling Program Leg 199, Site 1216, south of the Molokai Fracture Zone in the Central Pacific Basin.

The number of FMMNs changed drastically throughout the 40-m-long red clay intervals. FMMNs are abundant in the upper 9 m of core, decrease between 9 and 25 meters below seafloor (mbsf) with depth, and are very rare from 30 to 40 mbsf. Chemical composition of FMMNs showed high Mn/Fe ratios and Ni and Cu contents and a distinct positive Ce anomaly because of the existence of buserite. This suggests that FMMNs in the red clay from 25 mbsf to the top of the cored interval were deposited continuously in an oxic diagenetic bottom environment. The red clay below 30 mbsf with higher Mn contents contains few FMMNs but abundant tiny Mn particles within brown silicates coated by Fe (oxy-hydro)oxides. This indicates that the mode of manganese deposition changed between 25 and 30 mbsf.

INTRODUCTION

According to a study of temporal and spatial distributions of fossil ferromanganese micronodules (FMMNs) in sedimentary columns in the

¹Ito, T., Komuro, K., Hatsuya, K., and Nishi, H., 2005. Chemical compositions of ferromanganese micronodules in sediments at Site 1216, ODP Leg 199, Paleogene equatorial transect. *In* Wilson, P.A., Lyle, M., and Firth, J.V. (Eds.), *Proc. ODP, Sci. Results*, 199, 1–20 [Online]. Available from World Wide Web: <http://www-odp.tamu.edu/publications/199_SR/VOLUME/CHAPTERS/211.PDF>. [Cited YYYY-MM-DD]

²Faculty of Education, Ibaraki University, Mito, Ibaraki, 310-8512, Japan. tito@mx.ibaraki.ac.jp

³Institute of Geoscience, University of Tsukuba, Tsukuba, Ibaraki, 305-8572, Japan.

⁴Department of Earth and Planetary Sciences, Graduate School of Science, Hokkaido University, N10 W8, Sapporo, 060-0810, Japan.

world's oceans by Glasby (1978), the formation of FMMNs was intimately associated with the development of oxygen-rich bottom currents during the Cenozoic. The chemistry and mineralogy of FMMNs are related with bottom water depositional environments. According to Bonatti et al. (1972) and Dymond et al. (1984), ferromanganese deposits can be classified into four types (i.e., hydrogenous, oxic diagenetic, suboxic diagenetic, and hydrothermal) on the basis of chemical and mineralogical compositions. Chemical and mineralogical analysis for a series of fossil FMMNs from a successive sedimentary sequence is expected to provide key information about paleodeep-sea environments; however, it may be difficult to perform these analyses because FMMNs are present only rarely in sedimentary columns (Cronan, 1973; Aumento and MacGillivray, 1975; Menard, 1976; Glasby, 1978; Karpoff et al., 1980, 1985; De Carlo and Exon, 1992; Usui and Ito, 1994).

FMMNs, defined as ferromanganese nodules <1 mm in diameter, are distributed widely not only in the present seafloor but also in the sedimentary columns beneath the seafloor (e.g., Nakao and Mizuno, 1982; Sugisaki et al., 1987; Winter et al., 1997). It is expected that extraction and analysis of a series of FMMNs from a successive section will provide important information on their genesis and changes in the deep-sea environments. Here we describe distribution, morphology, chemistry, and mineralogy for FMMNs and heavy metal contents for host bulk sediment samples from a successive red clay section of Site 1216, with a discussion of the change of the sedimentary environments of the site during the Cenozoic era.

SAMPLES

Samples used in this study were collected in intervals of 1.5–4.7 m from the red clay of Site 1216. The site is located on abyssal hills south of the Molokai Fracture Zone (21°27.16'N, 139°28.79'W; water depth = 5163 m) (Fig. F1) (Shipboard Scientific Party, 2002). The lithology of the core comprises red clay from the top of the core to 50 meters below seafloor (mbsf) and interbedded clay with chert from 50 to 62 mbsf (Fig. F2). The depositional age of the red clay, determined by the paleomagnetic method, is considered to be middle Eocene to Holocene (Shipboard Scientific Party, 2002).

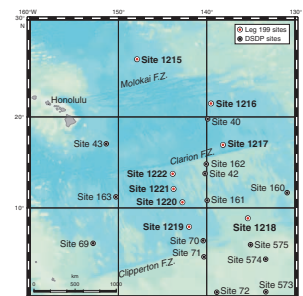
In bulk sediment chemistry, Si, Ca, Mg, P, and Sr are almost constant; Al and Ti decrease; and Fe, Mn, and Ba increase with depth (Shipboard Scientific Party, 2002). Shipboard pore water analyses showed very low Mn contents ranging from 2.1 to 3.9 μM in the red clay (Shipboard Scientific Party, 2002), showing that intensive reductive dissolution of manganese oxides and subsequent remobilization of manganese has not proceeded. These findings suggest that original depositional and early diagenetic signals have been well preserved in the FMMNs in the section.

PROCEDURES

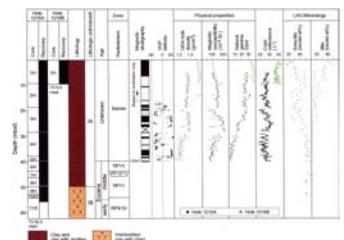
Each sample was separated into two parts for FMMN and bulk rock chemical analysis. The FMMN analysis was carried out after extraction.

FMMNs were extracted by magnetic separation for >25- μm fractions after wet screening. The screening was carried out with a small pouch of 25- μm nylon mesh in distilled water, which was stirred at least five

F1. Map of the central tropical Pacific, p. 9.



F2. Site 1216 lithologic summary, p. 10.



times over 3 days. The residual >25- μm fraction scattered on a glass dish was separated using a Sm-Nd magnet of 4000 G covered with a plastic cup. After air drying, the >25- μm magnetic fraction was weighed and was used for observational, chemical, and mineralogical analysis. The black particles, probably FMMNs, appeared to be well concentrated in this magnetic fraction.

Morphology, surface structure, and chemistry of the particles in the magnetic fraction were examined using a binocular microscope and a JEOL JMS-5400 scanning electron microscope with an electron dispersion spectrometer (SEM-EDS). The maximum sizes of FMMNs were measured under a binocular microscope.

X-ray diffraction (XRD) and chemical analyses by inductively coupled plasma–atomic emission spectroscopy (ICP-AES) and inductively coupled plasma–mass spectrometry (ICP-MS) were carried out for FMMNs, which were carefully hand picked from the >25- μm magnetic fraction under a binocular microscope. The hand-picked fraction was dried at 60°C overnight and was powdered using an agate mill. The powdered sample was completely dissolved in a mixture of concentrated acids—HNO₃ (0.1 mL), HClO₄ (0.05 mL), HF (0.25 mL), and HCl (0.1 mL)—in a closed Teflon vial at 105°C. The sample solution was dried in an open system at 200°C and made up in a final solution of 5% HNO₃. Chemical compositions were analyzed using ICP-AES (Jarrell Ash ICAP-757V) and (Yokogawa Hewlett Packard PMS2000) at the Chemical Analysis Center, the University of Tsukuba, Japan.

The procedure for chemical analysis of bulk sediment is almost identical to those for FMMNs except for the amounts of powdered sample (~60 mg) and the acids used (HNO₃ [0.5 mL], HClO₄ [0.2 mL], HF [1 mL], and HCl [0.2 mL]).

RESULTS

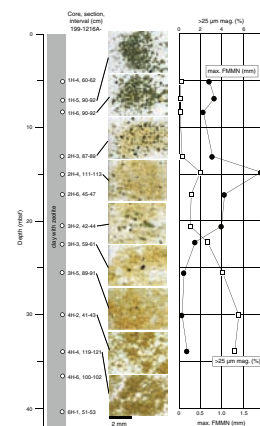
Magnetic Fractions of >25 μm

The proportion of the >25- μm magnetic fraction in Site 1216 sediments changes with depth (Fig. F3). The upper four samples (5.1–13.1 mbsf) have lower proportions ranging from 0% to 0.4%, and three samples from 14.8 to 20.6 m range from 1% to 2%. The lower four samples (30.1–40.2 mbsf) have higher proportions from 2% to 6%, showing an increase with depth.

On the basis of color, morphology, and structure under a binocular microscope, particles in the >25- μm magnetic fraction throughout the samples can be classified into three types: FMMNs, white silicates having black small particles of <10 μm , and brown silicates coated by Fe (oxy-hydro)oxides.

The proportion of these three types changes significantly with depth. FMMNs are abundant in the upper 9 mbsf of the core, decrease between 9 and 25 mbsf with depth, and are very rare from 30 to 40 mbsf. The size of FMMNs also varies significantly with depth (Fig. F3). The maximum size of FMMNs is >0.5 mm in diameter. Below 22 mbsf, the maximum size of the FMMNs is very small, only <0.2 mm in diameter (Fig. F3), in spite of high Mn contents in the sediments. White silicates having small black particles of <10 μm are rarely present from the top of the core to 25 mbsf and are barren below 25 mbsf. Brown silicates coated by Fe (oxy-hydro)oxides are present throughout the core, and the abundance increases with depth. In the magnetic fractions from 30

F3. Binocular microscopic photographs, p. 11.



to 40 mbsf, the brown silicates are the only dominant phase. SEM-EDS mapping for brown silicates from 30.11 mbsf demonstrates the existence of tiny Mn particles several micrometers in diameter (Fig. F4).

FMMNs

FMMNs were divided into types A and B based on color, shape, and surface structure under a binocular microscope. Type A FMMNs are dominant throughout the core.

Type A FMMNs have a spherical, spheroidal, or columnar shape with a rough but porous surface of grayish black color and a soft luster (Fig. F5; samples 1, 2, 5, 6). Type B FMMNs have a lumpy structure with a black, dull, smooth surface (Fig. F5; samples 3, 4, 7, 8). Many Type B FMMNs have one conspicuous flat plane as shown in sample 7 on Figure F5. In Type B, FMMNs with a columnar shape were not detected.

Qualitative SEM-EDS analyses suggest that Mn, Si, Al, Mg, Ca, K, and Ni are dominant for Type A, and Mn, Fe, Si, Al, Mg, Ca, and Ti are dominant for Type B. Type A FMMNs have higher Ni and lower Fe and Ti contents than Type B FMMNs.

According to XRD analyses of Type A FMMNs from 5.10 and 17.15 mbsf, the former contain busserite with a peak at 9.7 Å and the latter is composed of birnessite with distinct peaks at 7.16 and 3.56 Å. Both samples have unidentified peaks at 4.78, 3.11, and 2.76 Å.

ICP-AES and ICP-MS analyses of Type A FMMNs from 6.90 and 8.40 mbsf show that both FMMNs have high Mn/Fe ratios of 8.3 and 14.4 and are enriched in Ni and Cu (Table T1). As shown in Figure F6, rare earth element (REE) contents in FMMNs are lower than those in bulk sediments. North American shale composite (NASC)-normalized REE patterns exhibit a distinct positive Ce anomaly and a faint positive Eu anomaly. We did not analyze Type B FMMNs on XRD, ICP-AES, and ICP-MS because of their poor abundance.

Chemical Composition of Sediments

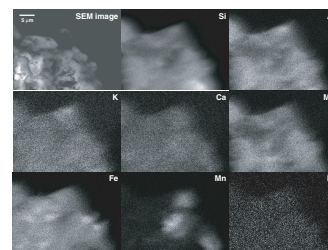
The chemical composition of bulk sediments is shown in Table T2. Profiles of Mn, Fe, Al, V, Ba, and Nd; ratios of Mn/Fe, Mn/Al, Ni/Mn × 100, and Cu/Mn × 100; and degrees of REE anomalies (Ce/Ce* and Eu/Eu*) are presented in Figure F7.

Mn content, Mn/Al ratios, and Eu/Eu* values increase with depth. Fe content is nearly constant above 22 mbsf and increases with depth below 26 mbsf. V content has a peak at 25 mbsf with a gradual decrease downhole. Ba content is constant above 25 mbsf and increases from 700 to 2700 ppm with depth. Nd content (as a representation of 3+REE), Mn/Fe, and Cu/Mn ratios show a broad peak in this sequence, but the horizons showing the maximum contents are different. Al content, Ni/Mn and Cu/Mn ratios, and Ce/Ce* decrease with depth.

Scatter plots of element contents vs. Mn, Fe, and P contents are shown in Figure F8. Elemental relationships of Mn vs. some elements vary ~2.4% in Mn content (Fig. F8), which corresponds to ~30 mbsf in the sediment column (Fig. F7). For example, two different scattered areas are distinguished in plots of Mn vs. P, Zn, Co, and Nd. Meanwhile, Mn shows continuously significant negative correlations with Al and Ce.

The elemental relationship between Fe and some element is discontinuous (Fig. F8). The elemental relationships vary ~8% in iron content, equivalent with ~25 mbsf, which is shallower than the boundary in the

F4. SEM-EDS mapping of the magnetic fraction, p. 12.

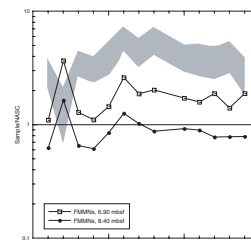


F5. SEM images of representative FMMNs, p. 13.



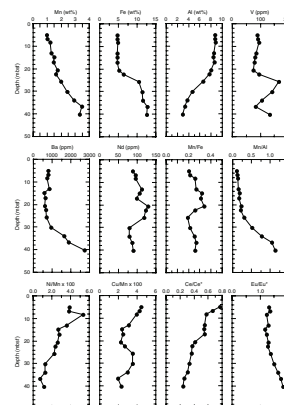
T1. Chemical composition of FMMNs, p. 19.

F6. NASC-normalized REE abundance of FMMNs, p. 14.



T2. Chemical composition of bulk sediments, p. 20.

F7. Elemental composition of bulk sediments, p. 15.



case of Mn. The interrelations of some elements vs. Mn and Fe in bulk sediment change at 30 and 25 mbsf, respectively.

NASC-normalized REE abundances are presented in Figure F9. Convex-upward REE patterns with negative Ce anomalies are characteristic of Site 1216 red clays. REE abundances and degrees of the anomalies correlate well with depth.

DISCUSSION

Origin of FMMNs

The foregoing analysis indicates the proportion of FMMNs in red clay with depth: FMMNs are abundant in the upper 9 mbsf and decrease with depth. The FMMNs are mainly of Type A with a small number of Type B. Type A has rough surface and is composed of birnessite and busserite, whereas Type B has smooth surface. Type A FMMNs are 8.3 and 14.4 in Mn/Fe ratio, 3.3 and 4.5 wt% in Ni content, and 0.80 and 1.05 wt% in Cu content (Table T1).

Higher Ni and Cu contents are characteristic of ferromanganese oxide composed of busserite and originating in oxic diagenesis (Dymond et al., 1984). The positive Ce anomaly (Fig. F6) is also characteristic of busserite (Elderfield et al., 1981). We consider the FMMNs from Site 1216 to have been formed in an under oxic diagenetic environment, although the Ni contents and Mn/Fe ratios are out of the range of published data (average = 1.4 ± 0.2 and 4.7 ± 1.2 , respectively) (Dymond et al., 1984; Calvert et al., 1987).

Sources of Metals in Sediments

The red clay below 30 mbsf with higher Mn content contains few FMMNs but abundant tiny (several micrometers) Mn particles within brown silicates coated by Fe (oxy-hydro)oxides (Fig. F4). There is no simple correlation between the number of FMMNs and Mn-Fe content in bulk sediment. This indicates a different mode of deposition for manganese below 30 mbsf.

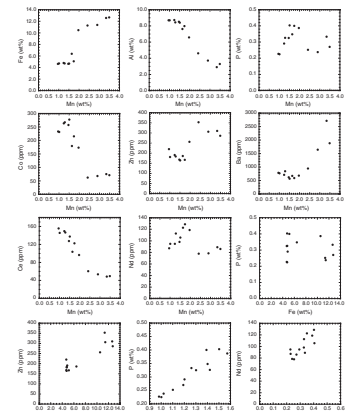
The bulk sediment chemistry of Site 1216 is plotted in Figure F10, which is a diagnostic diagram distinguishing marine sediments of different origins (Meylan et al., 1981). Six surficial samples are plotted around the terrigenous end-member sediment composition, and four samples below 20 mbsf with high Mn and Fe contents are included within the region of hydrothermal sediments (Fig. F10). The four samples below 30 mbsf are also enriched in Ba and Zn, which are well known to enrich hydrothermal deposits of active ridge crests (e.g., Bostrom and Peterson, 1969; Ruhlin and Owen, 1986). It is suggested that elemental input in the sedimentary column below 30 mbsf might originate from hydrothermal activity.

CONCLUSIONS

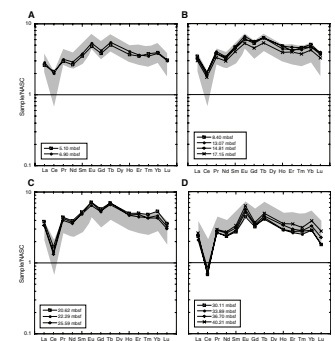
Studies of FMMNs and their host sediments from ODP Leg 199, Site 1216, produced the following conclusions:

1. The number of FMMNs changed significantly throughout the 40-m-long red clay section. FMMNs were commonly present

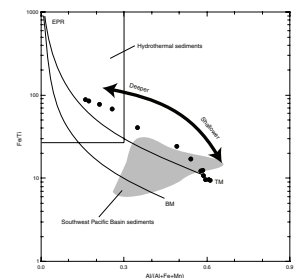
F8. Element concentrations of bulk sediments, p. 16.



F9. NASC-normalized REE abundances, p. 17.



F10. Fe/Ti vs. Al/(Al + Fe + Mn) plots, p. 18.



from 25 mbsf to the top of the sediment column, especially above 9 mbsf. The chemical composition of FMMNs showed high Mn/Fe ratios, high Ni and Cu contents, and a distinct positive Ce anomaly, which are all characteristic of buserite. This suggests that Fe-Mn deposition under oxic diagenetic bottom environment was continuous from 25 mbsf to the top of the core.

2. Only a sporadic presence of FMMNs was shown in the core from 30 to 25 mbsf in spite of higher Mn and Fe contents than the overlying succession. A series of analytical data in addition to high Mn and Fe contents supports a sedimentary environment effected by hydrothermal activity. This suggests that adequate Mn and Fe supply is not a necessary condition for FMMNs formation.

ACKNOWLEDGMENTS

This research used samples provided by the Ocean Drilling Program (ODP). ODP is sponsored by the U.S. National Science Foundation (NSF) and participating countries under management of Joint Oceanographic Institutions (JOI), Inc.

We appreciate technical help for extraction of FMMNs from Dr. T. Noguchi and for XRD analysis from Dr. M. Nakata. Drs. V.K. Banakar and K. Sugitani are gratefully acknowledged for their constructive reviews. Sincere thanks are expressed to Dr. M. Lyle for his helpful comments and precise handling.

Funding for this research was provided by a Grant-in-Aid for Scientific Research Projects from the Ministry of Education, Culture, Sports and Technology of Japan (number 14740297).

REFERENCES

- Aumento, F., and MacGillivray, J.M., 1975. Geochemistry of buried Miocene–Pleistocene ferromanganese nodules from the Antarctic Ocean. In Hayes, D.E., Frakes, L.A., *Init. Repts. DSDP*, 28: Washington (U.S. Govt. Printing Office), 795–803.
- Bonatti, E., Kraemer, T., and Rydell, H., 1972. Classification and genesis of submarine iron-manganese deposits. In Horn, D.R. (Ed.), *Papers from a Conference on Ferromanganese Deposits on the Ocean Floor*: Washington (Natl. Sci. Found.), 149–166.
- Boström, K., and Peterson, M.N.A., 1969. The origin of aluminium-poor ferromanganean sediments in areas of high heat flow on the East Pacific Rise. *Mar. Geol.*, 7:427–447.
- Calvert, S.E., Piper, D.Z., and Baedeker, P.A., 1987. Geochemistry of the rare earth elements in ferromanganese nodules from DOMES Site A, northern equatorial Pacific. *Geochim. Cosmochim. Acta*, 51:2331–2338.
- Cronan, D.S., 1973. Manganese nodules in sediments cored during Leg 16, Deep Sea Drilling Project. In van Andel, T.H., Heath, G.R., *Init. Repts. DSDP*, 16: Washington (U.S. Govt. Printing Office), 605–608.
- De Carlo, E.H., and Exon, N.F., 1992. Ferromanganese deposits from the Wombat Plateau, northwest Australia. In von Rad, U., Haq, B.U., et al., *Proc. ODP, Sci. Results*, 122: College Station, TX (Ocean Drilling Program), 335–345.
- Dymond, J., Lyle, M., Finney, B., Piper, D.Z., Murphy, K., Conard, R., and Pisias, N., 1984. Ferromanganese nodules from MANOP Sites H, S, and R—control of mineralogical and chemical composition by multiple accretionary processes. *Geochim. Cosmochim. Acta*, 48:931–950.
- Elderfield, H., Hawkesworth, C.J., Greaves, M.J., and Calvert, S.E., 1981. Rare earth element geochemistry of oceanic ferromanganese nodules and associated sediments. *Geochim. Cosmochim. Acta*, 45(4):513–528.
- Glasby, G.P., 1978. Deep-sea manganese nodules in the stratigraphic records: evidence from DSDP cores. *Mar. Geol.*, 28:51–64.
- Haskin, L.A., Haskin, M.A., Frey, F.A., and Wildeman, T.R., 1968. Relative and absolute terrestrial abundances of the rare earths. In Ahrens, L.H. (Ed.), *Origin and Distribution of the Elements*: New York (Pergamon), 889–912.
- Karpoff, A.M., Bourbon, M., Ancel, B., and de Graciansky, P.C., 1985. Diagenetic polymetallic crusts at Sites 550 and 548 of Leg 80, northeastern Atlantic ocean. In de Graciansky, P.C., Poag, C.W., et al., *Init. Repts. DSDP*, 80: Washington (U.S. Govt. Printing Office), 823–844.
- Karpoff, A.M., Peterschmitt, I., and Hoffert, M., 1980. Mineralogy and geochemistry of sedimentary deposits on Emperor Seamounts, Site 430, 431, and 432: authigenesis of silicates, phosphates and ferromanganese oxides. In Jackson, E.D., Koizumi, I., et al., *Init. Repts. DSDP*, 55: Washington (U.S. Govt. Printing Office), 463–489.
- Menard, H.W., 1976. Time, chance, and the origin of manganese nodules. *Am. Sci.*, 64:519–529.
- Meylan, M.A., Glasby, G.P., Knedler, K.E., and Johnston, J.H., 1981. Metalliferous deep-sea sediments. In Wolf, K.H. (Ed.), *Handbook of Strata-Bound and Stratiform Ore Deposits* (Vol. 9): Amsterdam (Elsevier), 77–178.
- Nakao, S., and Mizuno, A., 1982. Regional sedimentologic data: in the central Pacific Wake-Tahiti transect, GH80-1 cruise. In Mizuno, A., and Nakao, S. (Eds.), *Regional Data of Marine Geology, Geophysics, and Manganese Nodules: the Wake-Tahiti Transect in the Central Pacific, January–March 1980 (GH80-1 Cruise)*. Cruise Rep.—Geol. Surv. Jpn, 18:95–123.
- Ruhlin, D.E., and Owen, R.M., 1986. The rare earth element geochemistry of hydrothermal sediments from the East Pacific Rise: examination of a seawater scavenging mechanism. *Geochim. Cosmochim. Acta*, 50:393–400.

- Shipboard Scientific Party, 2002. Leg 199 summary. *In* Lyle, M., Wilson, P.A., Janecek, T.R., et al., *Proc. ODP, Init. Repts.*, 199: College Station TX (Ocean Drilling Program), 1–87.
- Sugisaki, R., Ohashi, M., Sugitani, K., and Suzuki, K., 1987. Compositional variations in manganese micronodules: a possible indicator of sedimentary environments. *J. Geol.*, 95:433–454.
- Usui, A., and Ito, T., 1994. Fossil manganese deposits buried within DSDP/ODP cores, Legs 1–126. *Mar. Geol.*, 119:111–136.
- Winter, B.L., Johnson, C.M., and Clark, D.L., 1997. Geochemical constraints on the formation of late Cenozoic ferromanganese micronodules from the central Arctic Ocean. *Mar. Geol.*, 138:149–169.

Figure F1. Map of the central tropical Pacific showing Leg 199 and DSDP drill sites (adapted from Shipboard Scientific Party, 2002). F.Z. = fracture zone.

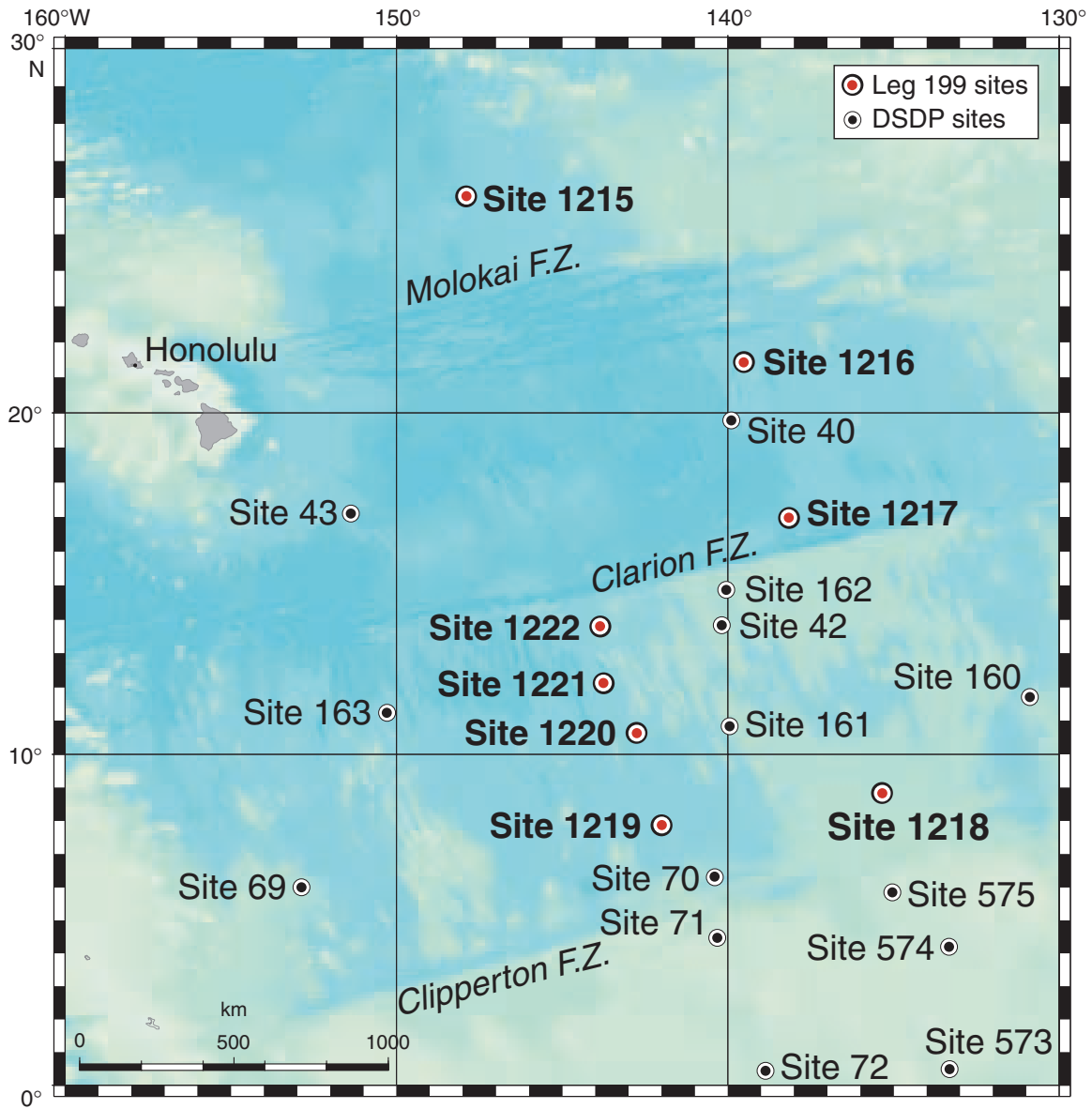


Figure F2. Lithologic summary for Site 1216 (adapted from Shipboard Scientific Party, 2002). VGP = virtual geomagnetic pole, GRA = gamma ray attenuation, LAS = light absorption spectroscopy, cps = counts per second, TD = total depth.

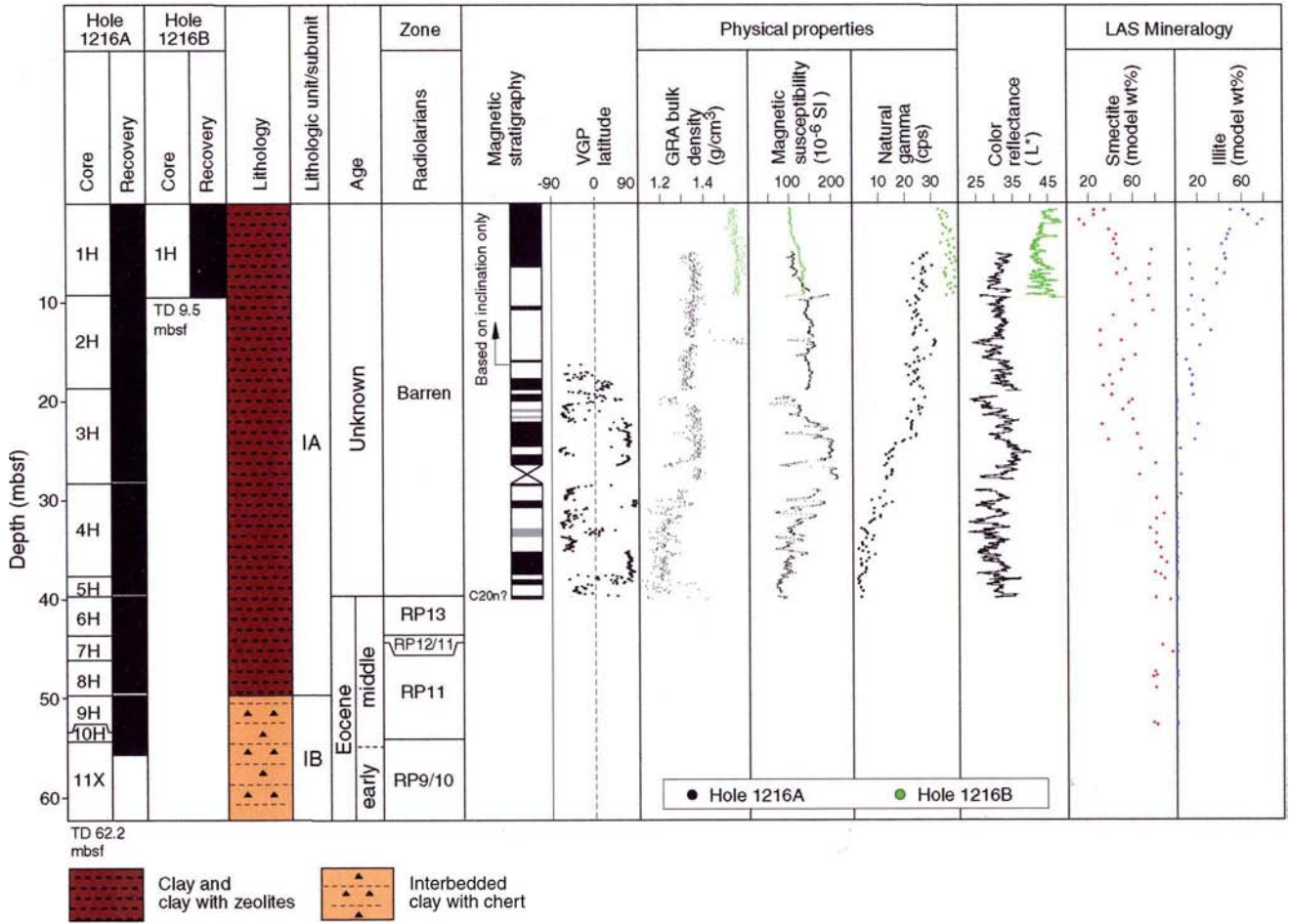


Figure F3. Binocular microscopic photographs, content of magnetic fraction (>25 μm in diameter), and maximum size of ferromanganese micronodules (FMMNs) at Site 1216. mag. = magnetic, max. = maximum.

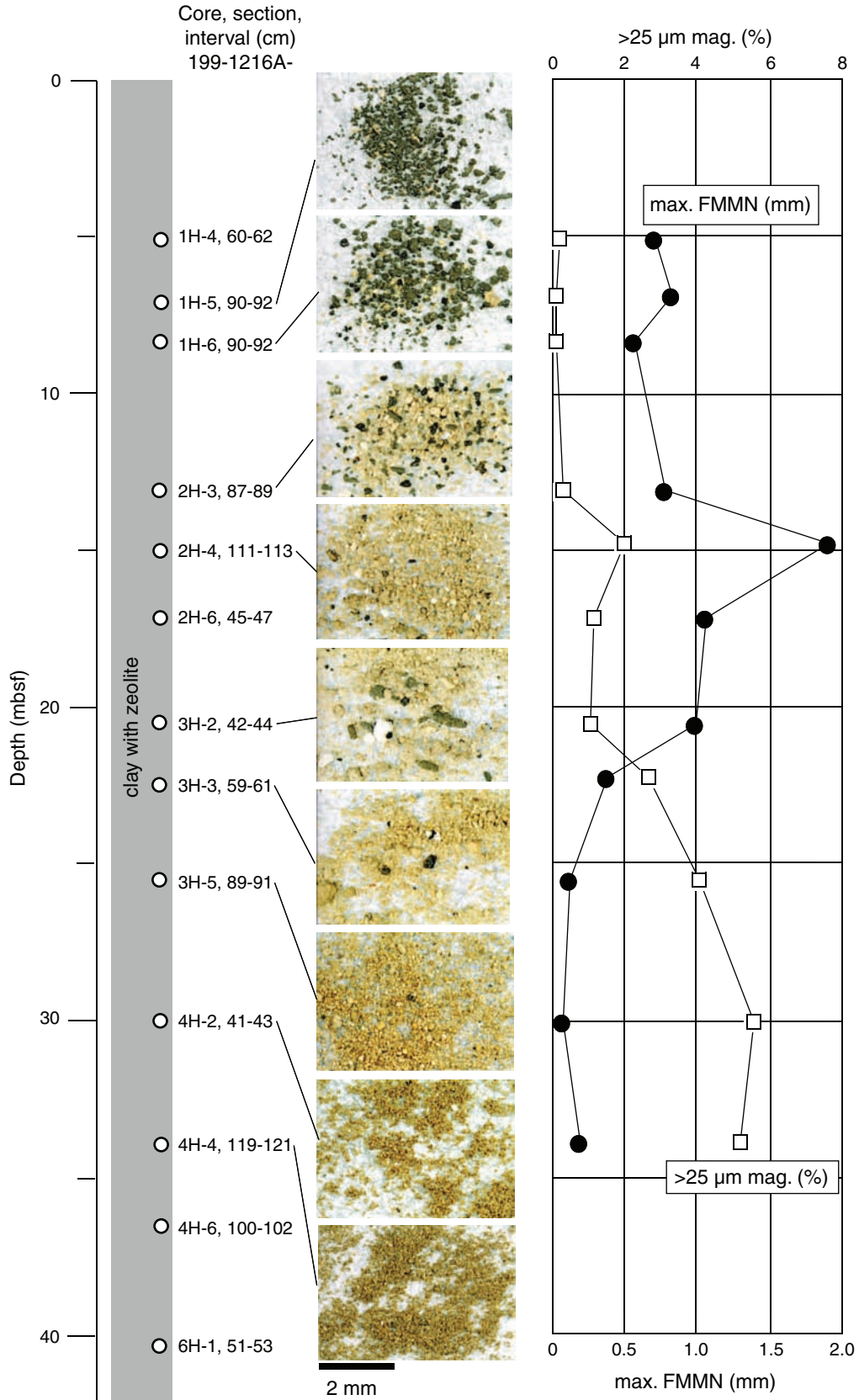


Figure F4. SEM-EDS mapping of the magnetic fraction (>25 μm in diameter) (Sample 199-1216A-4H-2, 41–43 cm; 30.11 mbsf).

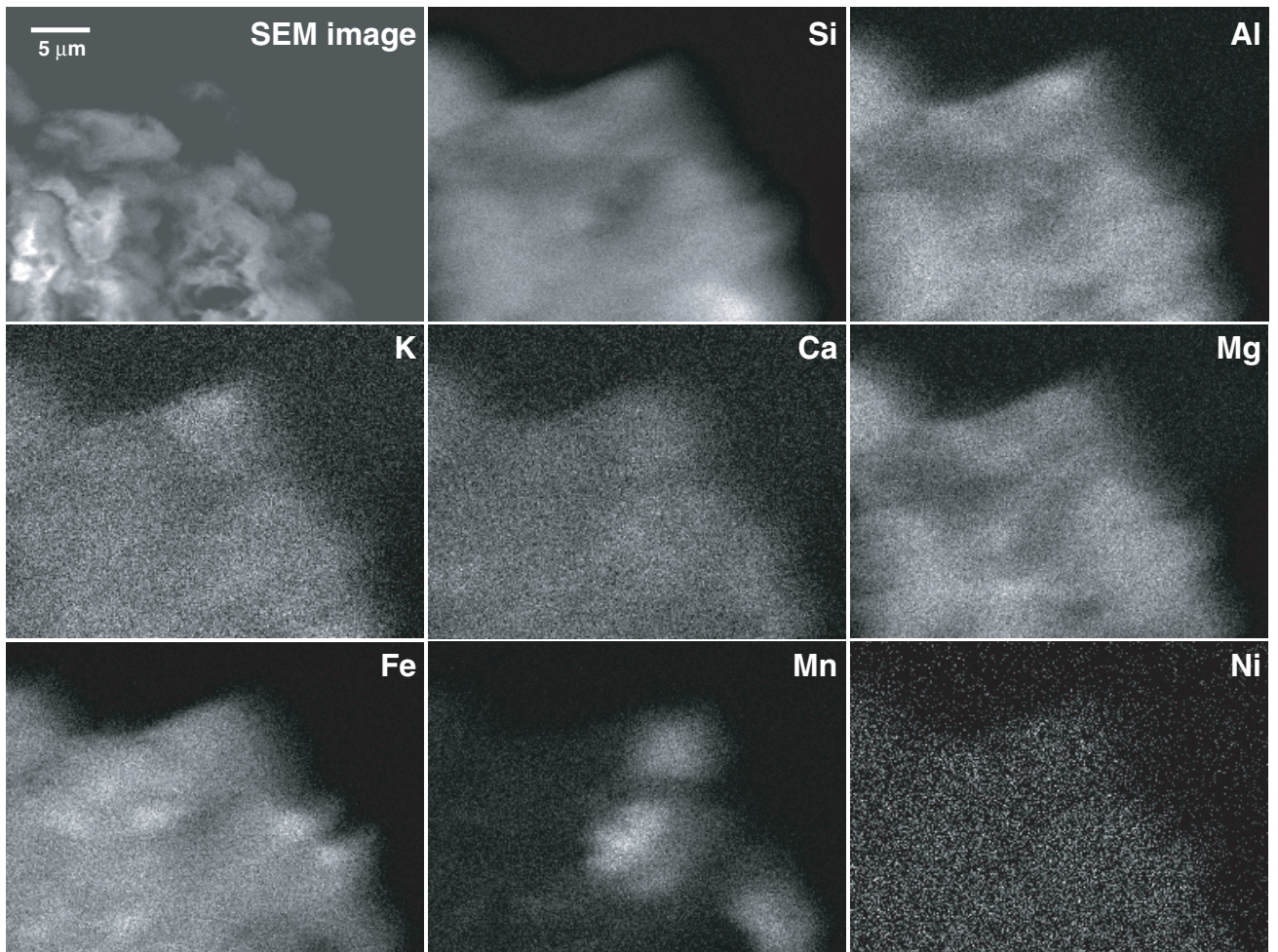


Figure F5. SEM images of representative ferromanganese micronodules (scale bar = 100 μm). 1–4. Sample 199-1216A-1H-4, 60–62 cm (5.1 mbsf). 5–8. Sample 199-1216A-2H-6, 45–47 cm (17.15 mbsf).

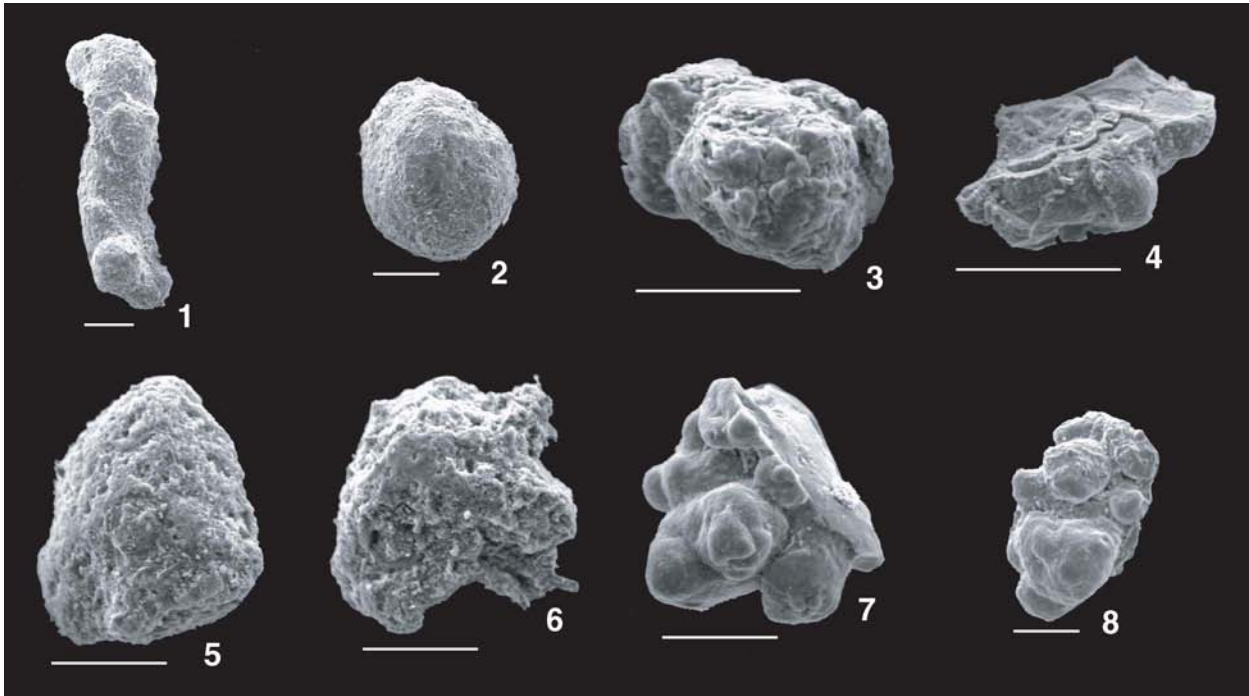


Figure F6. North American shale composite (NASC)-normalized REE abundance of ferromanganese micronodules (FMMNs), Site 1216. NASC data are adapted from Haskin et al. (1968). The shaded area represents the range of REE abundance of bulk sediment samples.

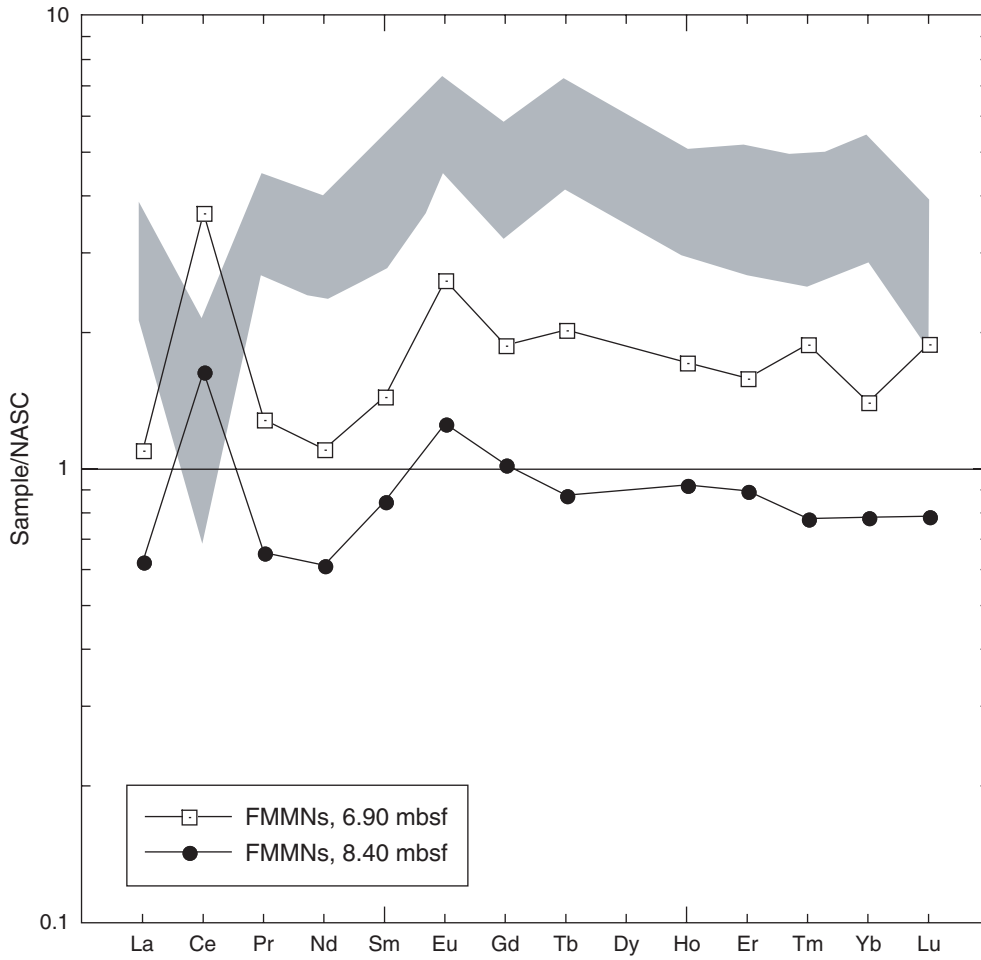


Figure F7. Elemental composition of bulk sediments from Site 1216. The Ce and Eu anomalies are defined as $Ce/Ce^* = (2Ce_{ANALYSIS}/Ce_{NASC}) / (La_{ANALYSIS}/La_{NASC} + Pr_{ANALYSIS}/Pr_{NASC})$ and $Eu/Eu^* = (2Eu_{ANALYSIS}/Eu_{NASC}) / (Sm_{ANALYSIS}/Sm_{NASC} + Gd_{ANALYSIS}/Gd_{NASC})$. North American shale composite (NASC) data are adapted from Haskin et al. (1968), and ANALYSIS shows analytical data.

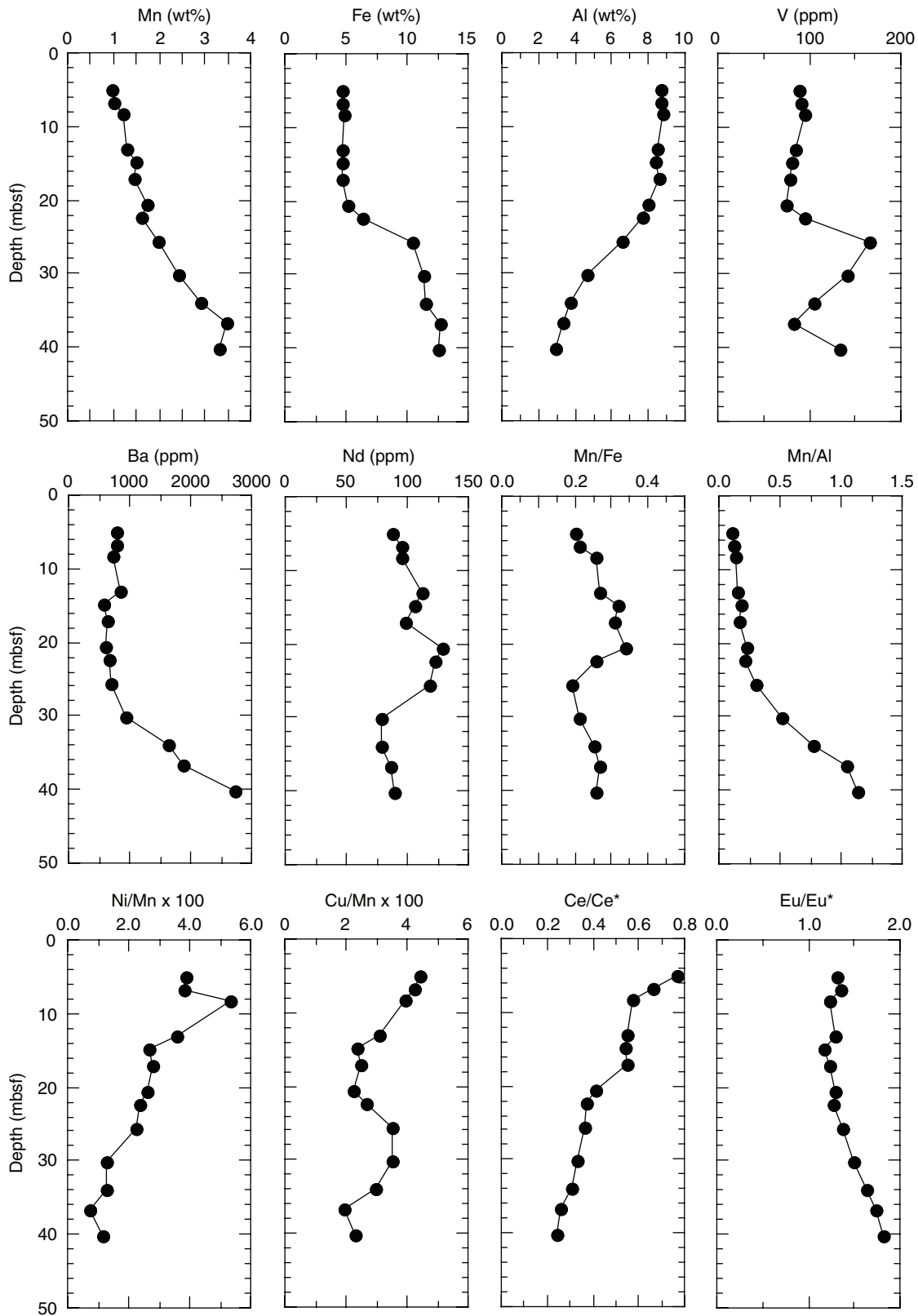


Figure F8. Scatter plots of element concentrations of bulk sediment samples, Site 1216.

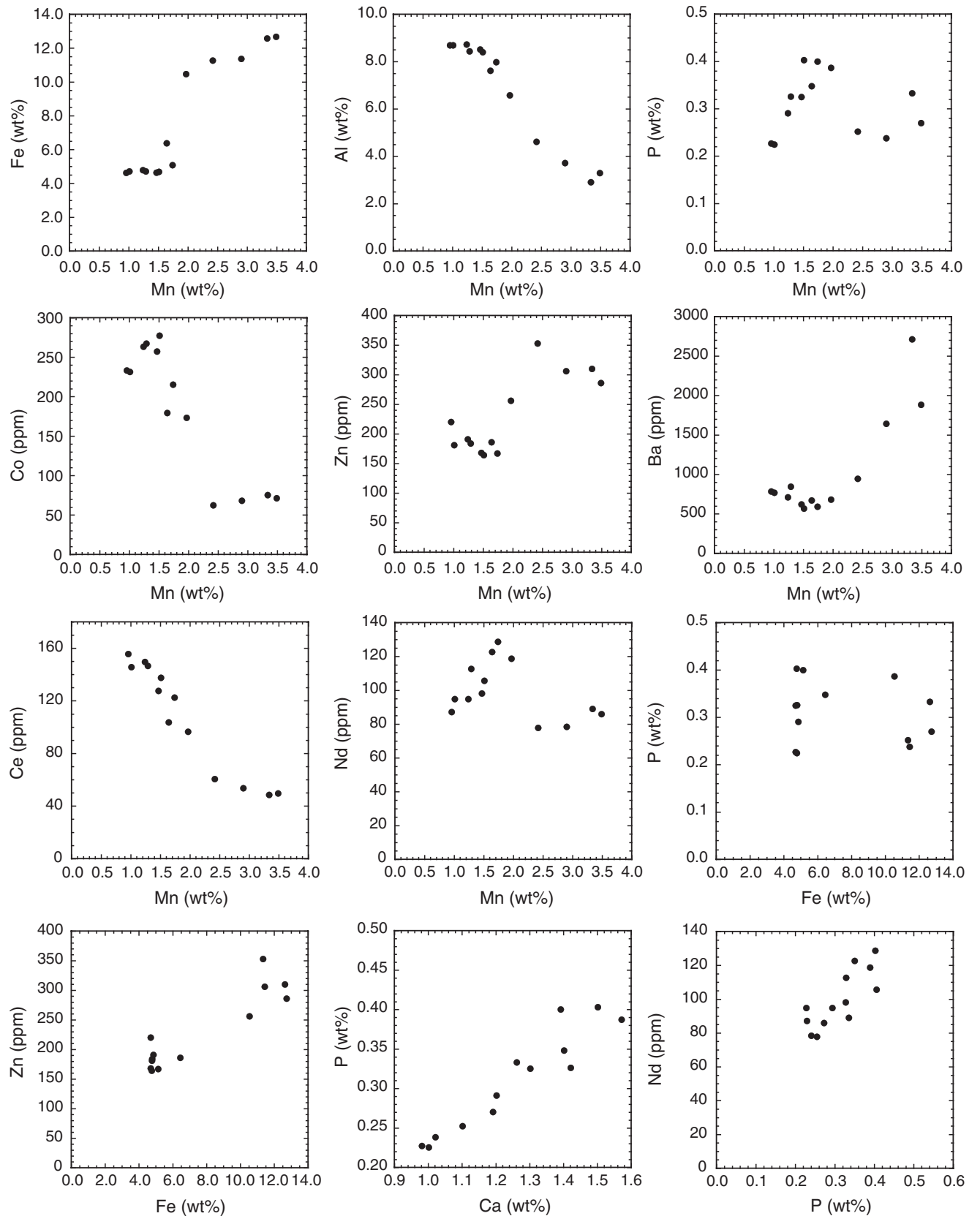


Figure F9. North American shale composite (NASC)-normalized REE abundance of bulk sediment samples, Site 1216. The shaded fraction represents the range of REE abundance.

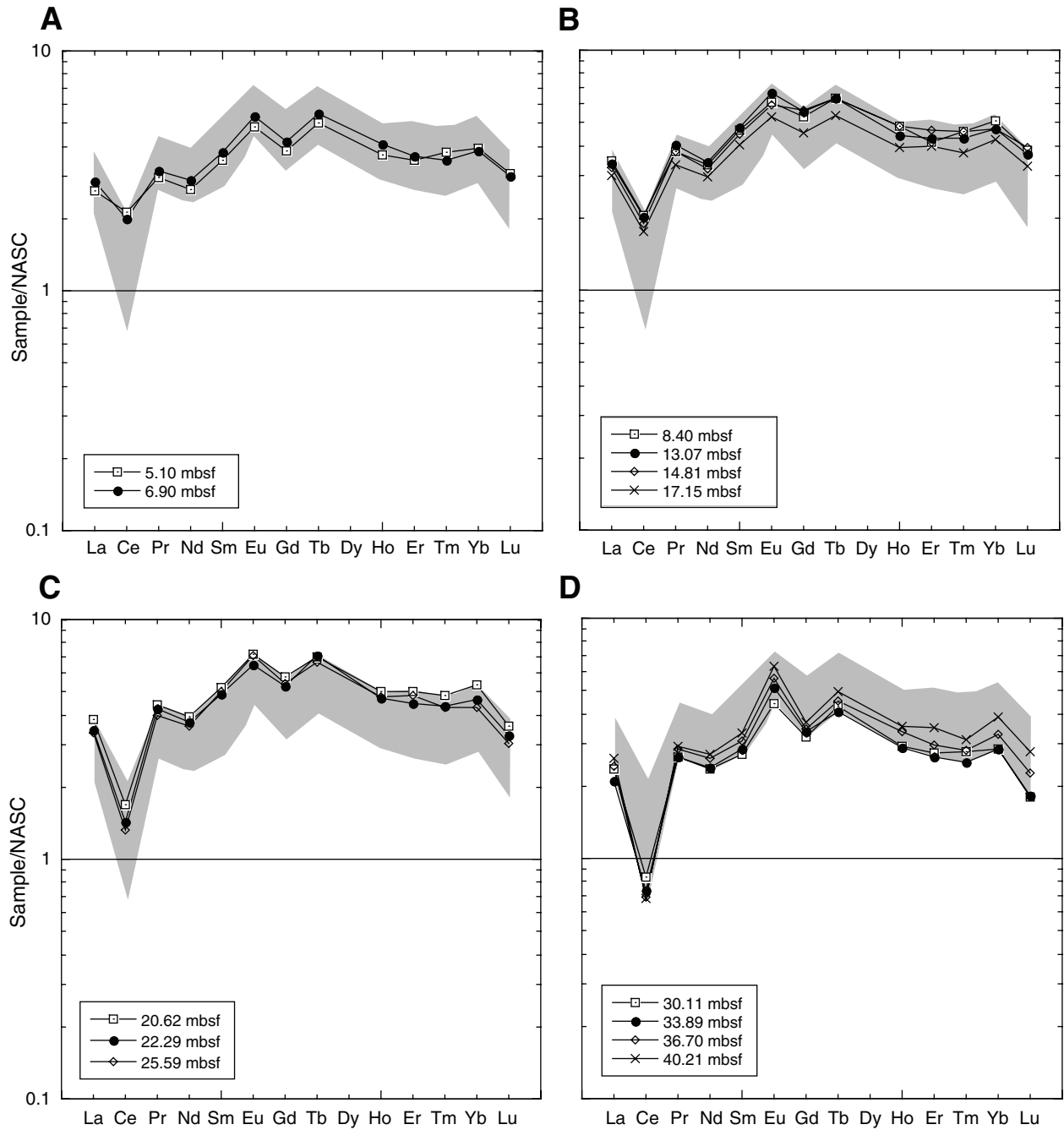


Figure F10. Fe/Ti vs. Al/(Al + Fe + Mn) plots for bulk sediments, Site 1216. BM = biogenic matter end-member sediment composition, EPR = East Pacific Rise hydrothermal end-member sediment composition, TM = terrigenous matter end-member sediment composition (Meylan et al., 1981).

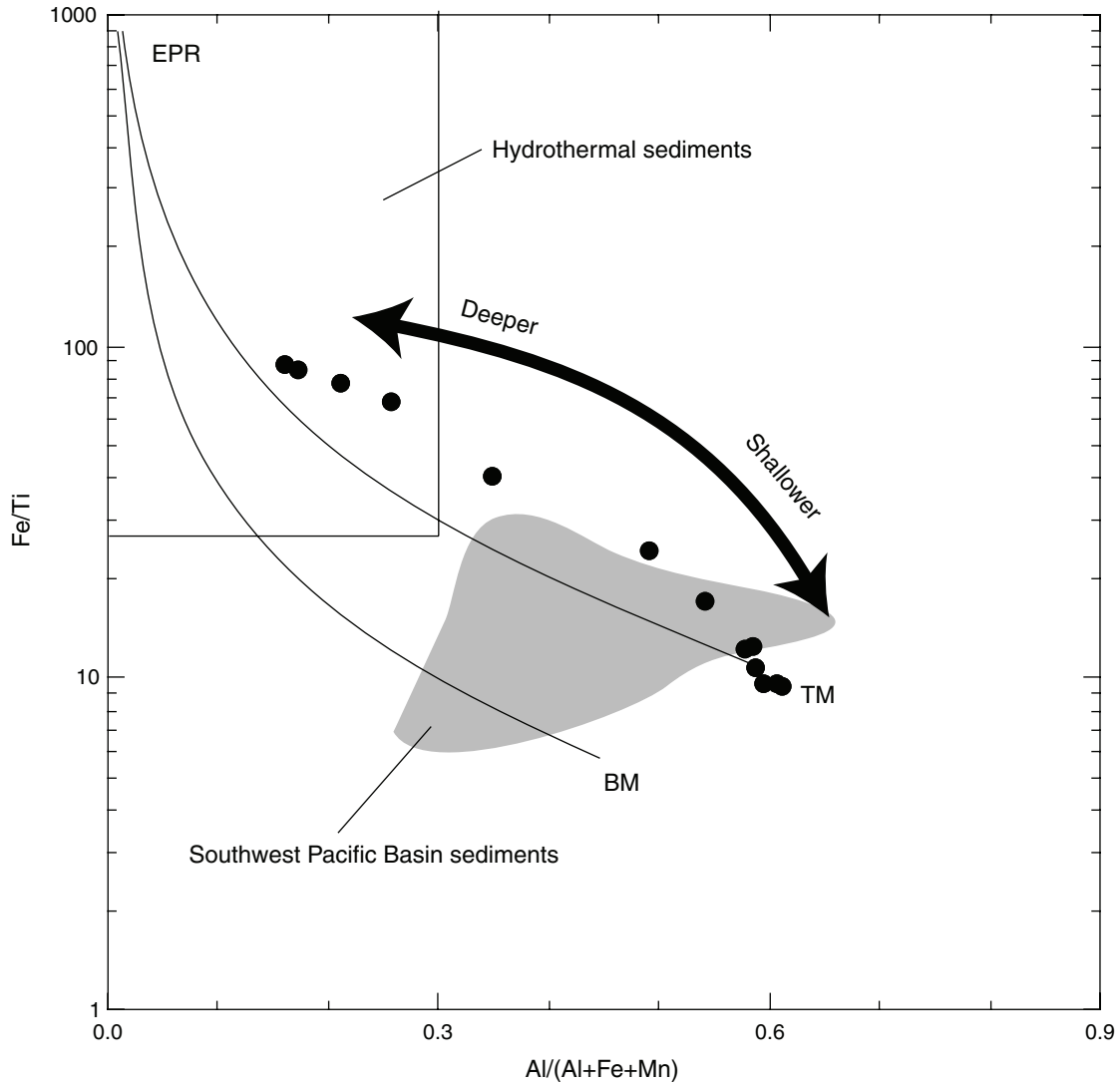


Table T1. Chemical composition of FMMNs, Site 1216.

Core, section, interval (cm):	199-1216A-	
	1H-5, 90-92	1H-6, 90-92
Depth (mbsf):	6.90	8.40
Element:		
Li (ppm)	47.0	50.3
Be (ppm)	3.66	0.73
Na (wt%)	0.61	0.64
Mg (wt%)	2.77	3.03
Al (wt%)	4.10	3.38
P (ppm)	885	469
K (wt%)	4.50	2.46
Ca (wt%)	1.60	1.70
Sc (ppm)	7.04	3.58
Ti (wt%)	0.241	0.170
V (ppm)	126	81
Cr (ppm)	52.4	17.0
Mn (wt%)	25.8	30.7
Fe (wt%)	3.11	2.13
Co (ppm)	2000	1240
Ni (wt%)	3.29	4.47
Cu (wt%)	0.80	1.05
Zn (ppm)	1380	1439
Ga (ppm)	90.3	63.8
Ge (ppm)	23.5	19.4
As (ppm)	43.4	38.8
Rb (ppm)	34.6	20.0
Sr (ppm)	281	258
Y (ppm)	47.1	27.0
Zr (ppm)	83.2	44.2
Nb (ppm)	9.19	4.84
Mo (ppm)	142	108
Ag (ppm)	4.35	2.22
Cd (ppm)	4.79	3.37
In (ppm)	2.34	0.52
Sn (ppm)	0.47	0.34
Sb (ppm)	4.53	6.59
Te (ppm)	2.21	1.60
Cs (ppm)	4.44	1.64
Ba (ppm)	554	261
La (ppm)	35.3	20.0
Ce (ppm)	268	120
Pr (ppm)	10.2	5.18
Nd (ppm)	36.5	20.3
Sm (ppm)	8.25	4.84
Eu (ppm)	3.24	1.57
Gd (ppm)	9.76	5.33
Tb (ppm)	1.73	0.74
Dy (ppm)	8.61	4.59
Ho (ppm)	1.79	0.96
Er (ppm)	5.40	3.05
Tm (ppm)	0.94	0.39
Yb (ppm)	4.36	2.43
Lu (ppm)	0.91	0.38
Hf (ppm)	2.34	1.25
Ta (ppm)	0.84	0.14
W (ppm)	15.0	9.7
Tl (ppm)	32.1	60.1
Pb (ppm)	106	52.5
Bi (ppm)	5.33	1.39
Th (ppm)	6.40	2.09
U (ppm)	3.34	0.74

Note: FMMNs = ferromanganese micronodules.

Table T2. Chemical composition of bulk sediments, Site 1216.

Core, section, interval (cm):	199-1216A-												
	1H-4, 60-62	1H-5, 90-92	1H-6, 90-92	2H-3, 87-89	2H-4, 111-113	2H-6, 45-47	3H-2, 42-44	3H-3, 59-61	3H-5, 89-91	4H-2, 41-43	4H-4, 119-121	4H-6, 100-102	6H-1, 51-53
Depth (mbsf):	5.10	6.90	8.40	13.07	14.81	17.15	20.62	22.29	25.59	30.11	33.89	36.70	40.21
Element:													
Li (ppm)	36.7	37.0	35.5	28.6	23.9	23.7	19.2	18.6	21.0	41.4	35.8	24.0	19.1
Be (ppm)	2.63	2.07	2.70	2.55	2.30	2.19	2.85	2.08	2.89	2.71	2.44	2.50	2.93
Na (wt%)	3.07	3.04	3.05	3.65	4.14	4.09	4.17	4.08	3.54	3.90	4.17	3.87	3.71
Mg (wt%)	1.70	1.75	1.73	1.46	1.27	1.26	1.26	1.34	1.54	2.36	2.46	2.32	2.22
Al (wt%)	8.71	8.71	8.75	8.46	8.42	8.54	8.00	7.64	6.60	4.64	3.74	3.32	2.93
P (wt%)	0.228	0.226	0.292	0.327	0.404	0.326	0.401	0.349	0.388	0.253	0.239	0.271	0.334
K (wt%)	4.10	4.09	3.98	4.27	4.66	4.69	4.99	4.30	3.10	1.76	1.78	1.82	1.94
Ca (wt%)	0.98	1.00	1.20	1.42	1.50	1.30	1.39	1.40	1.57	1.10	1.02	1.19	1.26
Sc (ppm)	24.9	27.4	27.4	25.0	22.2	21.3	24.1	21.2	21.9	11.2	11.6	11.9	12.3
Ti (wt%)	0.476	0.482	0.485	0.430	0.377	0.362	0.291	0.258	0.253	0.160	0.142	0.147	0.138
V (ppm)	88.6	91.6	95.5	84.6	80.3	78.5	74.6	95.9	165	142	105	83.2	133
Cr (ppm)	72.1	63.7	65.1	46.0	40.7	36.5	39.8	26.2	30.1	31.7	28.8	31.4	32.7
Mn (wt%)	0.95	1.00	1.23	1.28	1.50	1.46	1.73	1.63	1.96	2.41	2.89	3.48	3.33
Fe (wt%)	4.66	4.74	4.82	4.75	4.72	4.67	5.11	6.41	10.5	11.3	11.4	12.7	12.6
Co (ppm)	234	232	264	268	278	258	216	180	174	63	69	72	76
Ni (ppm)	368	383	654	455	396	405	451	390	439	300	364	255	382
Cu (ppm)	417	427	485	400	353	363	386	438	689	844	858	669	769
Zn (ppm)	221	182	192	185	165	169	168	187	257	354	307	287	311
Ga (ppm)	63.0	62.2	59.2	62.5	44.2	45.1	43.1	45.1	45.9	58.4	90.9	104.8	153.4
As (ppm)	12.2	11.5	12.0	12.9	15.0	13.7	15.1	21.0	36.1	26.6	18.3	15.4	22.4
Rb (ppm)	64.0	63.8	59.2	49.3	44.6	42.3	41.0	32.8	25.8	16.7	16.2	17.5	19.7
Sr (ppm)	261	247	258	272	259	245	225	230	258	230	240	325	333
Y (ppm)	110	114	141	135	137	123	157	140	139	79	75	86	98
Zr (ppm)	145	148	158	156	164	154	144	132	166	88	76	69	73
Nb (ppm)	18.6	17.3	16.0	14.8	15.5	13.2	11.9	11.6	9.4	7.0	6.3	4.2	3.5
Mo (ppm)	18.1	18.6	21.9	30.5	31.2	30.5	30.2	36.4	50.4	47.5	29.5	18.3	14.3
Cs (ppm)	7.56	7.49	7.57	5.94	4.56	3.96	4.21	3.10	3.00	2.39	2.14	1.95	2.30
Ba (ppm)	791	775	719	853	575	628	599	678	689	953	1,650	1,890	2,720
La (ppm)	84	91	110	107	104	96	123	110	108	76	67	78	84
Ce (ppm)	156	146	150	147	138	128	123	104	97	61	54	50	49
Pr (ppm)	23.3	25.1	29.8	31.8	30.0	26.4	34.7	33.4	31.5	20.9	20.9	22.4	23.1
Nd (ppm)	87.5	95.1	95.1	113	106	98.5	129	123	119	78.1	78.8	86.3	89.4
Sm (ppm)	20.0	21.5	26.4	27.0	25.4	22.9	29.6	27.9	28.5	15.5	16.4	17.7	18.9
Eu (ppm)	5.98	6.66	7.54	8.20	7.36	6.59	8.86	8.05	8.83	5.47	6.37	7.02	7.84
Gd (ppm)	20.0	21.7	27.3	28.8	29.2	23.5	30.0	27.4	28.1	16.6	17.6	17.9	19.2
Tb (ppm)	4.28	4.69	5.36	5.38	5.37	4.54	5.97	6.05	5.64	3.63	3.49	3.83	4.22
Dy (ppm)	19.2	20.8	23.7	23.3	21.7	20.8	26.1	23.3	24.1	14.2	13.8	14.9	18.2
Ho (ppm)	3.86	4.28	5.01	4.62	5.04	4.10	5.19	4.87	4.97	3.04	3.01	3.50	3.71
Er (ppm)	11.9	12.3	14.1	14.6	15.7	13.5	17.1	15.3	16.5	9.3	8.9	10.1	11.9
Tm (ppm)	1.89	1.75	2.30	2.15	2.28	1.88	2.40	2.18	2.14	1.39	1.25	1.40	1.57
Yb (ppm)	12.2	11.9	15.8	14.5	14.6	13.1	16.7	14.4	13.4	8.9	8.8	10.2	12.1
Lu (ppm)	1.49	1.45	1.85	1.78	1.89	1.58	1.72	1.57	1.46	0.87	0.87	1.09	1.33
Tl (ppm)	1.37	2.56	3.66	1.58	1.17	1.09	1.47	2.39	3.14	2.56	3.81	2.25	2.70
Pb (ppm)	40.4	34.1	37.6	35.7	39.1	37.9	40.2	39.9	56.5	51.6	61.6	73.6	74.9
Th (ppm)	14.7	12.1	11.8	11.1	12.3	11.9	11.3	11.1	7.2	8.3	4.8	3.2	2.3
U (ppm)	2.7	3.3	3.9	7.8	7.7	6.3	6.5	5.2	15.5	6.8	5.8	7.2	7.6